P-doped diamond grown on (110)-textured microcrystalline diamond: growth, characterization and devices

2009 J. Phys.: Condens. Matter 21 364204

(http://iopscience.iop.org/0953-8984/21/36/364204)

J. Phys.: Condens. Matter **21** (2009) 364204 (10pp) doi:10.1088/0953-8984/21/36/364204

P-doped diamond grown on (110)-textured microcrystalline diamond: growth, characterization and devices

Ken Haenen[1,2], Andrada Lazea[1,2], Julien Barjon[3], Jan D'Haen[1,2], Nada Habka[3,4], Tokuyuki Teraji[5], Satoshi Koizumi[5] and Vincent Mortet[1,2]

[1] Institute for Materials Research (IMO), Hasselt University, Wetenschapspark 1, B-3590 Diepenbeek, Belgium
[2] Division IMOMEC, IMEC vzw, Wetenschapspark 1, B-3590 Diepenbeek, Belgium
[3] Groupe d'Etude de la Matière Condensée (GEMaC), Université de Versailles St Quentin—CNRS, 1 place Aristide Briand, F-92195 Meudon Cedex, France
[4] Diamond Sensor Laboratory, LIST, CEA/Saclay, Bâtiment 451, F-91191 Gif-sur-Yvette, France
[5] Sensor Materials Center, National Institute for Materials Science (NIMS), 1-1 Namiki, Tsukuba, Ibaraki 305-0044, Japan

E-mail: ken.haenen@uhasselt.be

Received 5 April 2009, in final form 13 May 2009
Published 19 August 2009
Online at stacks.iop.org/JPhysCM/21/364204

Abstract
The formation and properties of (110)-textured P-doped microcrystalline CVD diamond were studied. Based on several microscopy techniques, with a special emphasis on electron backscattered diffraction, a detailed determination of the grain orientations with respect to the exact [110] axis is given. The different orientations present in the film, in combination with low phosphine concentrations in the gas phase, lead to a variation in P incorporation that can vary over three orders of magnitude, as determined with cathodoluminescence mapping. The role of the surface morphology in the observation of these large incorporation differences is explained. Hall measurements confirm that the films are n-type conductive with a thermal activation energy of 0.56 eV. Based on B-doped substrates, pn junctions were created, showing a rectification ratio of nearly 10^4 at ± 25 V.

(Some figures in this article are in colour only in the electronic version)

1. Introduction

The use of diamond as the next-generation wide bandgap semiconductor for bipolar devices requires controllable and reproducible p-and n-type dopants. Notwithstanding a multitude of efforts in search for a shallow donor, the only well-established donor atom that has been found to date is phosphorus. Investigations with many different experimental techniques have proven that the donor level is situated at 0.56 eV under the conduction band [1, 2]. Over the years, many theoretical investigations have predicted a plethora of shallow doping levels, based on incorporation of single elements, like sulfur or arsenic [3], or even complexes involving at least two different elements [4]. The literature contains several reports based on experimental evidence that sulfur and a boron–deuterium complex yield n-type conduction with donor ionization energies of 0.38 eV [5] and 0.23 eV [6], respectively, but these results remain controversial because of the difficulties in reproducing them.

In contrast to this, successful investigations by several groups on different oriented substrates and making use of several precursor gasses have reinforced the fact that phosphorus is at present the only viable n-type dopant [7–11]. Reproducible and efficient n-type doping of CVD diamond with phosphorus on (111)-and (001)-oriented homoepitaxial diamond has been successfully achieved since 1997 [7] and 2005 [8], respectively. Despite a common deposition temperature of about 900 °C, other deposition parameters differ

substantially. While (111) substrates require a very low $[CH_4]/[H_2]$ ratio of 0.05% and $[PH_3]/[CH_4]$ ratios of the order of 100–10 000 ppm, (001)-oriented films are optimally grown using a 0.4% methane-to-hydrogen ratio. However, the latter requires an unusually large amount of the P-containing gas phosphine to reach sufficient doping levels. It is not uncommon to use 5% or higher of PH_3 with respect to the methane concentration, immediately indicating one of the remaining problems when (001) substrates are used, i.e. a very low doping efficiency of only 0.02%. In addition, a substantial amount of compensation of the P donor is found. The rationale behind the use of this orientation is the fact that the highest quality B-doped films, needed to construct bipolar devices, are grown on (001) diamond substrates. In contrast, (111) films still show a lower compensation ratio, typically around 7%, in combination with a larger attainable doping window that was recently enlarged, making it now possible to reproducibly obtain doping levels ranging between 1×10^{16} and 1.2×10^{20} cm^{-3} [12, 13]. Even so, the large difference in P-doping efficiency and compensation ratio for these two orientations shows that the substrate orientation plays a significant role that is not fully understood to date.

In the n-type diamond-based device field, a lot of progress has been made in the fabrication of uni-and bipolar devices since the first report on UV emission from a diamond pn junction by Koizumi *et al* in 2001 [14]. Schottky diodes and pin structures have been successfully fabricated on (111)- as well as on (001)-oriented homoepitaxially grown diamond films, even yielding rectification ratios of 10^{10} at ± 25 V at room temperature [15]. Regardless of this, a widespread application of such devices is still hampered by price issues and limitations in size. Currently, polycrystalline diamond has regained a lot of attention, especially when its grain size is limited, creating so-called nanocrystalline diamond or NCD. While polycrystalline B-doped diamond is already well established, from thick, freestanding microcrystalline discs [16] to very thin (∼100 nm) nanocrystalline films [17], a thoroughly studied n-type counterpart is lacking [18].

In this work, (110)-textured microcrystalline CVD diamond films were used as a substrate on which to deposit P-doped films. As all the grains from the substrate show a certain misorientation with respect to the perfect crystallographic [110] axis, they form an ideal starting point to further elucidate the role of the substrate orientation on the P-incorporation efficiency in the separate grains. After all, growth experiments on such substrates, which were polished before P-doped epitaxial growth, can be considered similar to a situation in which as many monocrystalline substrates with different miscut angles are used as there are grains in the microcrystalline substrates. Recently, Lazea *et al* have shown that it is possible to successfully incorporate P in such homoepitaxial layers by applying specific doping conditions [19, 20]. In well-defined cases, a combination of cathodoluminescence spectroscopy and electron backscattered diffraction (EBSD) can yield spatial information on the phosphorus concentration [P] as a function of the grain orientation. Special emphasis will be put on the role of the surface morphology. The n-type character of the layers will be discussed based on Hall effect measurements. As a last step, the possibility to use such layers in combination with polished B-doped microcrystalline substrates for pn-junction fabrication will be investigated.

Table 1. Conditions used for the fabrication of the (110)-textured CVD diamond substrates.

Deposition parameter	Undoped substrates	B-doped substrates
Source gases	CH_4, H_2	CH_4, H_2, TMB
$[CH_4]/[H_2]$ (%)	3	3
$[TMB]/[H_2]$ (ppm)	—	100
Microwave power (W)	6000	6000
Total gas pressure (Torr)	110	100
Total gas flow (sccm)	500	500
Substrate temperature (°C)	850–900	850–900
Growth duration (h)	550	300
Layer thickness (mm)	∼1.2	∼0.4
Growth rate (μm h^{-1})	∼2.2	∼1.3

2. Experimental details

All substrates used were microcrystalline CVD diamond discs initially grown on (001) silicon substrates of 2 inches in diameter. Undoped, as well as boron-doped, material was deposited, both grown in an ASTeX 6500 steel chamber type reactor, based on growth conditions given in table 1. The boron precursor gas was trimethylborane (TMB) with a purity of 99.5% (2.5N) diluted in hydrogen of 99.9999% (6N) purity. The thickness of the substrate material ensured grain sizes of several tens to hundreds of micrometres. After deposition, the silicon substrate was removed, and 3 mm diameter substrates were cut by laser from the freestanding 2 inch Ø wafers, subsequently followed by polishing of the surface.

The P-doping epitaxy was carried out in an ASTeX PDS 17 system, using a molybdenum substrate holder placed on the water-cooled stage. Growth temperature during deposition was measured using a disappearing filament optical pyrometer from Pyrometer Instrument Co. Inc. The typical growth conditions can be found in table 2 [19]. The purity of the source gases used were 99.9999% (6N) for methane, and 99.999% (5N) for phosphine, which was diluted in 99.999 9999% (9N) pure H_2. The choice for these particular conditions was inspired by the work of Teraji *et al* who used higher than conventional methane concentrations and growth temperatures for the growth of high quality boron-doped homoepitaxial diamond [21]. Here, similar differences with respect to the well-established P-doping conditions for single-crystalline films can be found, as can be remarked from the introduction to this paper.

The film surface morphology and structure was studied with several microscopy techniques, including differential interference contrast microscopy (DICM) (Axiovert 40 MAT), atomic force microscopy (AFM) (Veeco NanoScope IIIa) and electron backscattered diffraction (EBSD). The latter is performed using an HKL Technology system installed in a scanning electron microscope (SEM) type Quanta 200-FEG manufactured by FEI. The typical penetration depth of the EBSD e-beam is several tens of nanometres, yielding the surface orientation of the different grains.

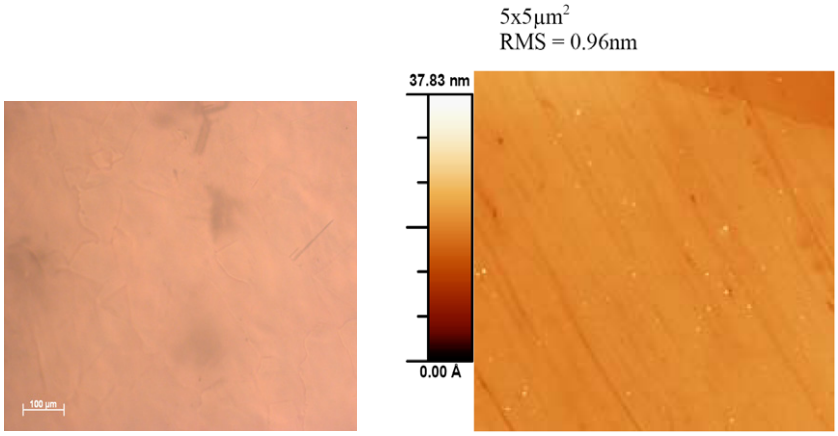

Figure 1. (a) DICM image and (b) AFM image of an undoped microcrystalline diamond substrate.

Table 2. Conditions used for the epitaxy of P-doped CVD diamond films on undoped or B-doped substrates.

Deposition parameter	Undoped substrates	B-doped substrates
Source gases	CH_4, H_2, PH_3	CH_4, H_2, PH_3
$[CH_4]/[H_2]$ (%)	1	1
$[PH_3]/[H_2]$ (ppm)	100–500	100
Microwave power (W)	600–700	600–700
Total gas pressure (Torr)	180	180
Total gas flow (sccm)	500	500
Substrate temperature (°C)	1140	1130
Growth duration (h)	2	2
Layer thickness (μm)	>20	>20
Growth rate (μm h^{-1})	>10	>10

P-incorporation was studied with cathodoluminescence (CL) spectroscopy and mapping at 102 K, performed with a Horiba Jobin Yvon SA system installed on a JEOL 840 scanning electron microscope. The P-doped diamond layers were excited with a 20 keV focused electron beam at a current of 0.1 μA, corresponding to a penetration depth of ∼2.8 μm. To evacuate electric charges, the epitaxial layers were coated with a semi-transparent gold layer (∼5 nm). The CL emission was collected by a parabolic mirror and injected with metal optics into a monochromator equipped with a UV enhanced-silicon CCD camera and a 600 grooves mm^{-1} diffraction grating. The CL maps were obtained by acquiring CL spectra scanning 32 × 32 or 64 × 64 points inside a 380 × 300 μm^2 or 60 × 45 μm^2 window, respectively.

The Hall set-up is equipped with a 0.7 T magnet for generating an AC magnetic field ($0.52T_{rms}$) with frequencies ranging from 10 to 200 mHz. During the experiments, the samples were placed in He ambient at a pressure of 1 Pa in a high temperature cryostat evacuated by a turbo molecular pump. Using this equipment, the specimen temperature can vary in a wide range, reaching a maximum value of 1073 K. A Keithley 6517A DC current source is used and the results are collected via a computer through custom-written Toyo Resitest 8310 software.

Metal contact deposition was carried out using a home-made sputtering system with a base pressure around 2 × 10^{-5} Pa. During deposition of aluminium or titanium, the carrier gas used was argon, at a pressure of 0.133 Pa. For the P-doped films, ∼100 nm Al was used to form ohmic contacts, while a stack of Ti (100 nm)/Al(100 nm) was deposited on the B-doped layers. After the metallization, all samples were annealed in high vacuum (∼10^{-6} Torr) at 450 °C for 45 min to ensure the stability of the deposited contacts during diode operation.

The $I(V)$ characteristics were measured through a custom-made LabVIEW program, at room temperature in air in dark surroundings with a 2400 Keithley Source Meter Unit. Wirebonded Al was used to connect the ohmic contacts of the pn junctions with the sample holder. The voltage was applied with respect to the electrode on the p-type layer.

3. Results and discussion

3.1. Surface topography and morphology

3.1.1. Substrates. To fully characterize the substrate material, the surface topography and morphology are first studied with DICM and AFM, as can be seen in figure 1. After polishing, the microcrystalline surface samples are macroscopically flat and microscopic defects due to the polishing procedure can be observed in the AFM image. The typical root mean square surface roughness (R_{rms}) as determined on a 5 × 5 μm^2 square part of the sample is around ∼1 nm.

To determine the orientation of the grains in the microcrystalline substrates, EBSD was used. As can be seen in figure 2(a), the {110} pole figure of a representative substrate proves that the texture is clearly (110), with no preferential orientation in-plane. The texture component image from figure 2(b) was taken with a step size of 20 μm, attributing a colour to each data point. Brighter colours correspond to grains whose orientation is closer to a perfectly oriented (110) plane parallel to the substrate, while darker grains have a larger miscut angle with respect to the surface normal. As can be

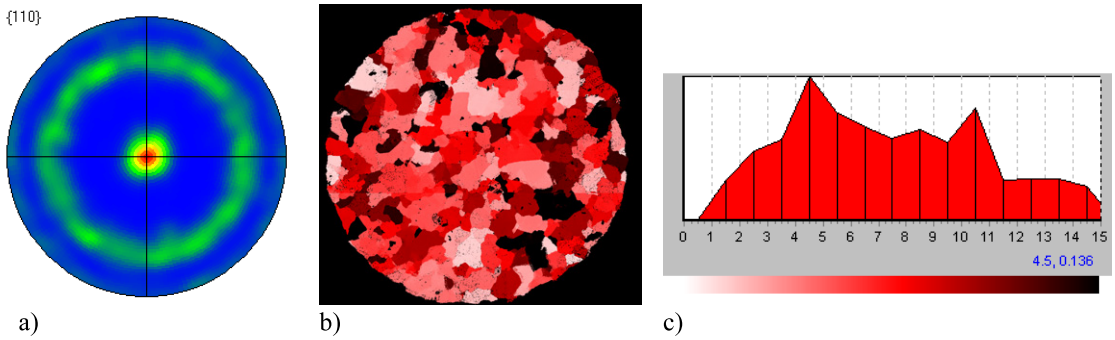

Figure 2. (a) {110} pole figure taken on a 3 mm Ø undoped diamond substrate, clearly showing a preferential (110) texture. (b) Corresponding (110) texture component image. The darker the grain colour, the higher the grain's misorientation angle with respect to the perfect [110] direction. (c) (110) texture component distribution corresponding to the image in (b), showing that most of the grains have a misorientation angle below 15°.

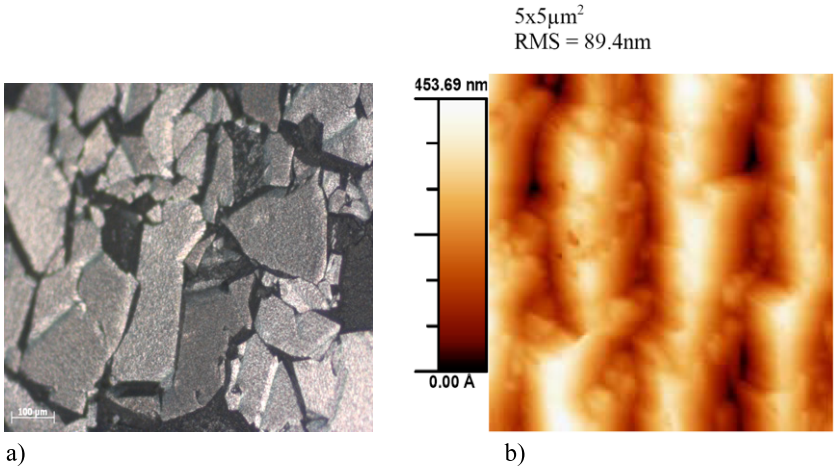

Figure 3. (a) DICM image and (b) AFM image of a P-doped microcrystalline diamond film after 2 h of growth with 500 ppm $[PH_3]/[CH_4]$.

seen, the majority of the grains have a misorientation angle below 15° with respect to a perfect [110] direction, a fact which is also reflected in the texture distribution of figure 2(c). These results were obtained on a complete 3 mm Ø substrate and are characteristic for all the substrates used for this work, i.e. undoped and B-doped.

3.1.2. P-doped films. After the growth of the P-doped layers with the deposition parameters given in table 2, the grown films were similarly characterized. The DICM image in figure 3(a) clearly shows that film deposition took place on all the grains, which is in contrast to the report of Nesládek *et al* where more conventional P-doping conditions were applied to grow P-doped polycrystalline diamond [18]. The AFM investigations (figure 3(b)) reveal a microscopically rough surface, with an average R_{rms} of ∼90 nm for a scan area of 5 × 5 μm^2. The noticeable increase in roughness is a result of the growth rate, which was estimated to be higher than 20 $\mu m\ h^{-1}$ based on the increase in film thickness after 2 h of growth.

When looking into more detail using EBSD images taken before and after plasma exposure, it can be established that homoepitaxial growth has taken place on each grain. Moreover, the overall grain orientation is not modified after the growth [19]. In figure 4 representative images are shown. Because of the epitaxial growth of the grains, with an increase of surface roughness as a result, the grain boundaries are now clearly visible in the image taken after a 2 h deposition run. Nevertheless, the overall colour of the map has not changed, confirming the unchanged (110) texture and the fact that all grains have grown under the presented conditions.

After growth, similar to the substrate case, all the grains of the P-doped film keep a certain misorientation, i.e. they are not perfectly (110)-oriented. This is well illustrated in figure 5. For this particular case, the substrate used was B-doped. Notice the smaller grain size when compared to figure 2(b). This can be explained by the smaller layer thickness of the B-doped substrates (∼0.4 mm) in comparison with the undoped films (∼1.2 mm). Despite this difference, the conclusion remains valid.

3.2. Cathodoluminescence and electron backscattered diffraction mapping

It has been known for a very long time that the incorporation of impurities in semiconductors, intentional or unintentional, can be very much dependent on the crystallographic orientation

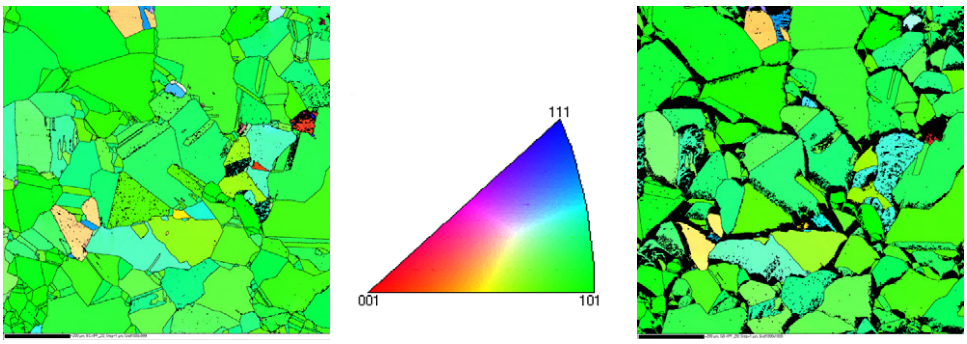

Figure 4. (a) 1 × 1 mm^2 EBSD inverse pole figure map of an undoped diamond substrate. (b) Legend explaining the colour codes used in (a) and (c). (c) 1 × 1 mm^2 EBSD inverse pole figure map of a ∼20 μm thick P-doped diamond film grown with 800 ppm [PH_3]/[CH_4].

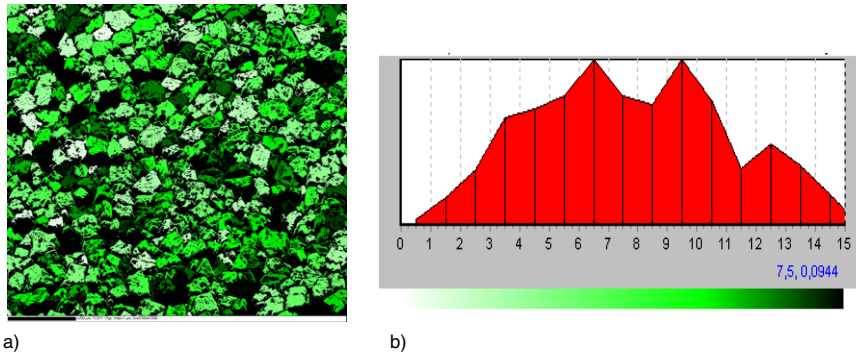

Figure 5. (a) 1 × 1 mm^2 (110) texture component image of a B-doped diamond substrate. The darker the grain colour, the higher the grain misorientation angle with respect to the perfect [110] direction. (b) (110) texture component distribution corresponding to the image in (a), showing that most of the grains have a misorientation angle below 15°.

of the substrate. For P-doping of diamond, efforts in that direction were mainly focused on the two most important planes, i.e. (111) and (001). It is very hard to polish diamond substrates with a perfect surface finish, keeping the orientation perfectly aligned with one of these two planes. As a result, the much used Ib HPHT diamonds usually show a certain misorientation with respect to the desired surface orientation, where a so-called off-angle is generally accepted. The best obtainable values are <0.5° for (001) and <3° for (111) surfaces. An increase of this misorientation can have a drastic influence on the growth mode observed [22] and, hence, also on the incorporation rate of the pursued impurity. Kato *et al* already pointed out that angles of 2° or 3° were helpful to enhance step flow growth and the subsequent phosphorus incorporation in (001) surfaces [23]. In the present case, the successful substitutional incorporation of P in the (110)-textured films was already proven by quasi-steady-state photocurrent (PC) measurements and cathodoluminescence spectroscopy at liquid nitrogen temperature. Using the CL technique, collecting light from the complete sample surface, it was shown that free as well as bound exciton luminescence was present, with an increase of the latter when the amount of PH_3 in the gas phase was increased [19]. By making use of the ratio of the free and P-bound exciton luminescence intensities Barjon *et al* [24, 25] have elegantly shown that it is possible to determine the active P concentration in CVD diamond. As a result, the combination of EBSD and CL mappings on microcrystalline diamond films can yield spatial information on the incorporation of P as a function of the substrate miscut orientation. Such data are valuable since they may be transposed to the case of homoepitaxial growth on single-crystalline diamond plates.

Figure 6(a) shows two CL spectra taken on two different areas of a film grown with 100 ppm [PH_3]/[CH_4] in the gas phase. These spectra show various exciton peaks, labelled TO or TA when assisted with a transverse optical or acoustic phonon, respectively, and NP in the case of a no-phonon transition [24–27]. Although both curves clearly show free (FE) and P-bound (BE_P) excitons, necessary to determine [P], there are obvious differences between them in intensity and linewidths of the signals. Whereas some places on the film yield spectra dominated by free exciton recombination (A), other areas exhibit a much larger bound exciton-related emission when compared to the free exciton signal (B). This visibly indicates a larger incorporation of substitutional phosphorus. What is more, the energetic positions of all exciton recombinations in spectrum B are shifted towards lower energies. This effect, which was already reported for P-doped films deposited directly on silicon [28], could indicate that a local bandgap reduction has taken place as a result of a large position-dependent tensile stress. The presence of strain inside the different grains is also coherent with the

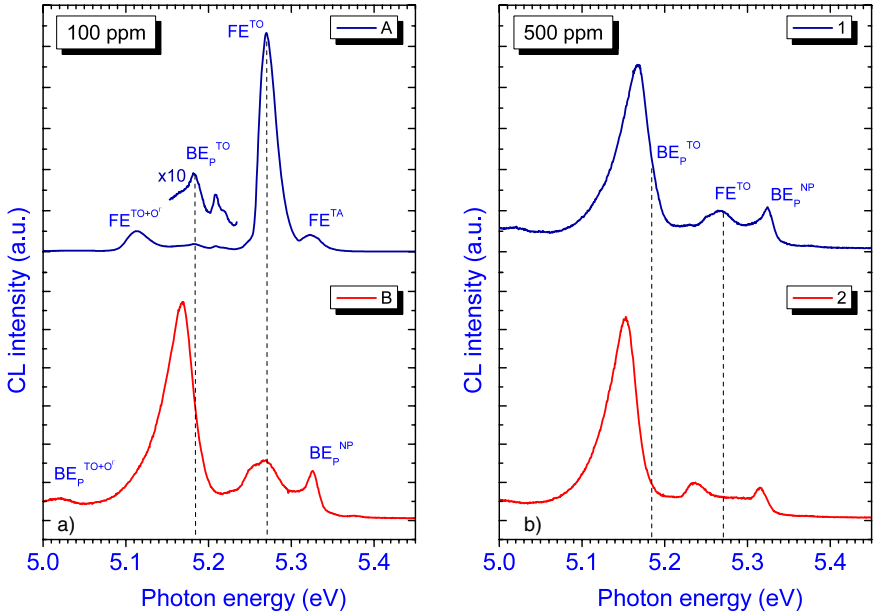

Figure 6. (a) Two CL spectra obtained at ∼100 K on a 100 ppm $[PH_3]/[CH_4]$-doped film. (b) Similar, but for a 500 ppm $[PH_3]/[CH_4]$-doped film. The dashed lines show where the free (FE) and P-bound (BE_P) exciton emissions are expected at 100 K for a stress-free film.

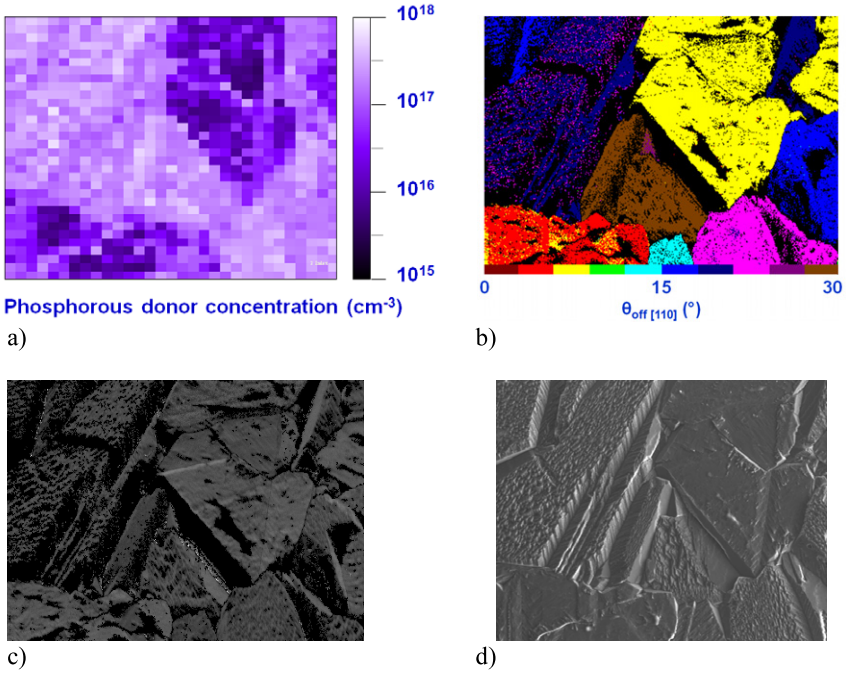

Figure 7. (a) 380 × 300 μm^2 P-concentration map based on the ratio of intensities of neutral phosphorus-bound exciton and free exciton emission as determined with CL mapping. The low concentration areas ($[P] < 10^{16}$ cm^{-3}) correspond typically to the 'A' CL spectrum of figure 6(a), while the high concentration areas ($[P] > 10^{17}$ cm^{-3}) correspond typically to the 'B' spectrum. (b) Corresponding EBSD map showing the miscut angle of the grains with respect to the exact [110] direction. The colour legend corresponds to off-angles between 0° and 30°, with a resolution of 3°. (c) EBSD surface image of the area depicted in (a) and (b). (d) SEM image of the area depicted in (a) and (b).

large BE_P^{TO} linewidths (43 meV) that can be observed. Such linewidths are well above those obtained for homoepitaxial layers (23 meV) [24, 25].

To further illuminate the local differences in P concentration in the 100 ppm $[PH_3]/[CH_4]$-doped film, the complete surface was mapped by CL. In figure 7(a), a typical result obtained on a 380 × 300 μm^2 area is shown. It becomes immediately clear that there is a large variation of [P], spanning three orders of magnitude with values ranging between 10^{15} and 10^{18} cm^{-3}. A corresponding EBSD map showing the misorientation angle $\theta_{off\ [110]}$ of the grains with respect to the surface normal, i.e. the perfect [110] direction, was made with a step size of

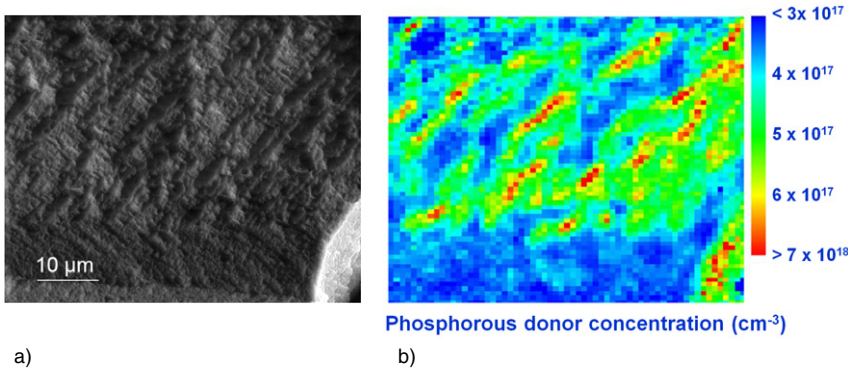

Figure 8. (a) SEM image taken on a 200 ppm $[PH_3]/[CH_4]$-doped film. (b) Corresponding P-concentration map based on the ratio of intensities of neutral phosphorus-bound exciton and free exciton emission as determined with CL mapping.

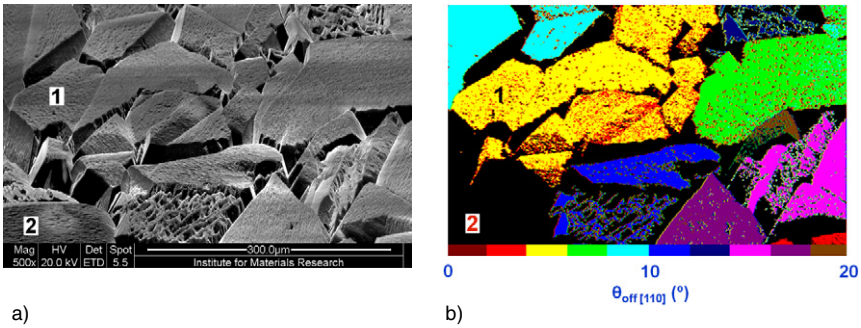

Figure 9. (a) SEM image taken on a 500 ppm $[PH_3]/[CH_4]$-doped film. (b) Corresponding EBSD map showing the misorientation angle of the grains with respect to the exact [110] direction. The colour legend corresponds to off-angles between 0° and 20°, with a resolution of 2°. The black regions are grains that are not included in the $0 \cdots 20°$ interval. The '1' and '2' correspond to CL spectra featured in figure 6(b).

1 μm to show the relationship with the grain orientation. Most of the grains fall within the 3°–24° interval, with a few showing larger misorientation. Comparing both figures, it becomes obvious that the P-incorporation efficiency is quite small for the red and yellow coloured grains, i.e. below 10^{16} cm^{-3}. The orientation of these grains falls in the 3°–9° interval, thus being closest to a perfect (110) plane in this film. Looking more carefully at figure 7(c), these grains also show a much smoother surface when compared to the rest of the film, where a certain roughness is present. Taking into account the micromorphology on the rougher grains (e.g. see also figure 3(b)), it is suggested that the more the grains are disoriented with respect to the [110] direction, the more they portray (111)-oriented microfacets [29]. As discussed in the introduction to this work, the incorporation efficiency of (111)-oriented layers is several orders of magnitude higher than for (100)-oriented films [23]. It is also accepted that growth on (110) faces is often stabilized through the formation of microfacets, which develop predominantly in (111) facets, leading to the rough appearance as seen in figure 7(c) [30, 31]. Moreover, calculations by Battaile *et al* point out that a certain misorientation can have a beneficial effect on the growth rate [32], enhancing locally the growth and subsequently the phosphorus incorporation of suitably oriented grains. Summarized, once the misorientation angle is large enough, i.e. >12°, microfacetting is favoured, resulting in an enhanced P concentration.

To investigate the influence of an increased phosphine concentration during the growth, samples with 200 and 500 ppm $[PH_3]/[CH_4]$ using identical conditions as the just-discussed film were made. For the 200 ppm sample, similar results could be obtained. Regions with low [P] and high [P] alternate, depending on the grain orientation, albeit that concentration interval is shifted to higher values than in the 100 ppm case. The importance of the microfacetting and the presence of growth steps for an enhanced P incorporation is again nicely illustrated in figure 8, supporting the earlier made assumptions. In addition, the overall roughness of the film increased, an effect which is completely attributed to the increased phosphine levels in the plasma. An argument to support this claim is found when looking at the CL spectra taken on the 500 ppm sample. As can be seen in figure 6(b), the typical CL signals taken on different areas of the film show a large BE_P^{TO} peak, with a much smaller free exciton-related emission. All grains show an incorporation of [P] > 10^{18} cm^{-3}, whatever the grain orientation. Contrary to the 100 and 200 ppm samples, looking at figure 9(a), all grains now show a surface with a high roughness, i.e. facets and growth steps that are being induced by the higher amount of phosphine; steps and facets which facilitate the impurity inclusion. Note that, despite the small differences in the BE_P^{TO}/FE intensity ratio for different areas of the film, both CL spectra show again severe stress-induced shifts in energy

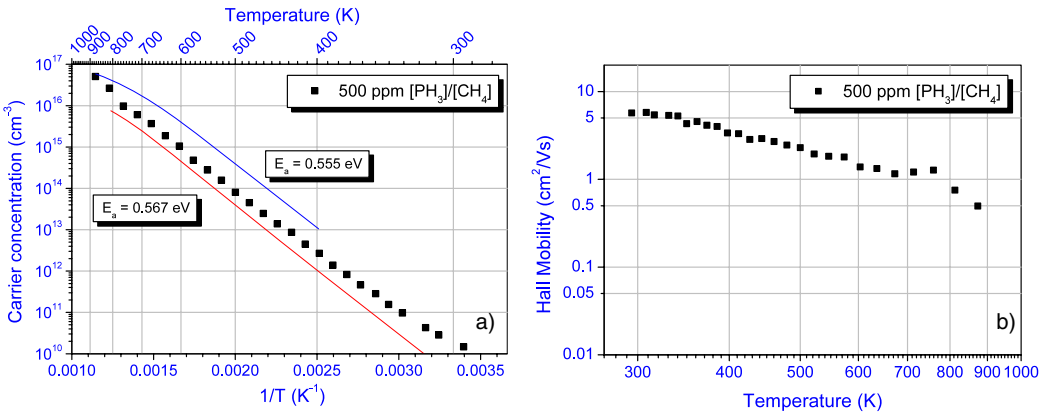

Figure 10. (a) Carrier concentration determined by van der Pauw Hall effect measurements on a 500 ppm [PH_3]/[CH_4]-doped film. (b) Corresponding Hall mobility. (c) Corresponding Hall mobility.

for the detected exciton signals. These findings could be confirmed with micro-Raman spectroscopy, where besides the well-known zone centre diamond line at 1332 cm^{-1}, a second downshifted peak could be detected. A detailed study combining CL and micro-Raman mapping carried out on the surface and cross section of the just-discussed 500 ppm doped sample is currently in the final stages and will be published elsewhere [33].

3.3. Transport properties

In the previous paragraphs, the successful incorporation of P into the (110)-textured film was proven. For a possible use in devices, it is of course necessary that the P atom acts as a donor and that n-type conductivity can be measured. To investigate the nature of the charge carriers governing the conduction in the layers, preliminary Hall measurements were applied in the van de Pauw configuration. The first results obtained on the 500 ppm doped sample confirm that the film is effectively n-type doped. The carrier concentration plot given in figure 10(a) illustrates an activation energy E_a of ∼0.56 eV, identical to the E_a obtained for single-crystalline P-doped films. For the entire temperature range, an exponential behaviour is seen, pointing to a conduction process that is governed by thermal activation of electrons into the conduction band.

Based on the same results, using a common procedure described, for example, in [23], one can calculate the compensation ratio $\eta = N_A/N_D$, yielding a value of nearly 30%. This value is about five times higher than the one reported for (111) single-crystalline diamond, but twice as low as that for (001)-oriented films. The Hall mobility at room temperature is ∼6 cm^2 V^{-1} s^{-1}, a value that is two orders lower than the highest reported values in the literature. Once more, this result is not surprising given the high P content of the film and the microcrystalline nature. At the moment, it is also not clear what the influence is of the surface roughness on the quality of the contacts used. Compared to single-crystalline layers, the roughness is much higher, posing a possible negative influence on the measured mobility values.

3.4. Pn junctions

To conclude this paper, the first results on pn junctions based on (110)-textured CVD diamond films are presented. For this purpose, 100 ppm [PH_3]/[CH_4] P-doped films of ∼20 μm were deposited on 0.4 mm thick 100 ppm [TMB]/[CH_4] B-doped substrates. The rather high thickness of the P-doped layer was chosen to ensure a closed layer on the B-doped substrate, avoiding any 'pinholes'. Contacts were applied on the top and bottom sides of this structure, followed by IV characterization. In figure 11 the result can be seen, showing

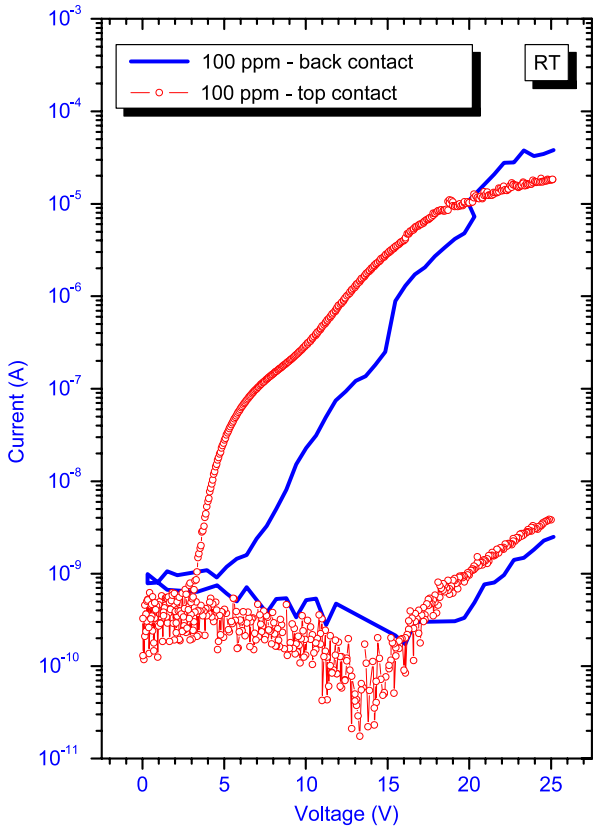

Figure 11. Room temperature $I(V)$ characteristics of two (110)-textured pn junctions based on 100 ppm [PH_3]/[CH_4] P-doped films of ∼20 μm grown on a 0.4 mm thick 100 ppm [TMB]/[CH_4] B-doped substrates. In the case of the curve labelled 'top contact', the P-doped layer was selectively grown on one-half of the B-doped substrate, leaving the other half exposed for contact formation from the top side.

a rectification ratio of nearly 10^4 at ± 25 V. Although this is six orders lower than the best result found in the literature for single-crystalline pin junctions on (001) substrates [15], it is an encouraging result. Despite this fact, the IV curve clearly shows a non-ideal behaviour with a high ideality factor. The turn-on voltage is higher than can be expected and there is a large influence of series resistance. Many factors can play a determining role, including contact resistance and the high resistivity values of the diamond layers. The formation of low resistive contacts on P-doped diamond is a difficult task that was only recently solved by Kato *et al* by the deposition of heavily phosphorus-doped diamond films with a phosphorus concentration of over 10^{20} cm^{-3}. In addition, the use of contacts on the top and back side of the pn structure forces the current to pass through 0.4 mm + 20 μm of diamond. From the Hall measurements, the room temperature resistivity value of the P-doped film was 7.4×10^7 Ω cm, a very high value. In an attempt to overcome this problem, a similar sample was grown, but this time one-half of the B-doped substrate surface was covered with a molybdenum plate during the P-doping plasma process. This method effectively led to a selective deposition of a P-doped layer on the non-covered half of the substrate. After metallizing the partly exposed B-doped layer from the top, i.e. at the same side as where the P-doped layer was contacted, the rectifying properties were studied again. The resulting IV curve now shows a much lower turn-on voltage and a steeper increase of the current when operated in forward mode. In order to enhance the rectification properties, future work will include an optimization of the doping levels, layer thickness and surface quality. Then, the UV photoresponse of the structures will be tested to compare them with single-crystalline structures, which are in high demand for UV detection in space research [34].

4. Conclusions

The growth of P-doped (110)-textured microcrystalline diamond was presented and discussed. A comprehensive structural and morphological investigation of the material was given, based on several microscopy techniques. The incorporation of phosphorus in the films was studied in detail by combing CL and EBSD mapping. When low phosphine concentrations are used, the local dopant incorporation can vary over three orders of magnitude, depending on the grain misorientation with respect to the perfect [110] direction. When this misorientation angle exceeds 10°, the formation of (111) microfacets occurs. These facets induce a significant roughening of the surface and enhance the P incorporation. Higher phosphine concentrations in the gas phase seem to accelerate this process, leading to a more evenly distributed [P] and a general rough appearance of all the grains. The shifts that are present in some of the CL spectra point to high levels of stress in some areas of the film. Next, the n-type nature of the films was shown using Hall effect measurements, demonstrating an activation energy of 0.56 eV, identical to the value obtained for P-doped single-crystalline layers. Finally, the suitability of these layers to form pn junctions with rectifying properties was shown. A rectification ratio of nearly 10^4 at ± 25 V was measured on non-optimized structures.

Acknowledgments

This work was financially supported by the EU FP6 Marie Curie RTN 'DRIVE' (MRTN-CT-2004-512224), the Research Programmes G.0068.07 and G.0430.07 of the Research Foundation—Flanders (FWO), the Methusalem 'NANO network' and the IAP-P6/42 project 'Quantum Effects in Clusters and Nanowires'.

References

[1] Haenen K, Meykens K, Nesládek M, Knuyt G, Stals L M, Teraji T, Koizumi S and Gheeraert E 2001 *Diamond Relat. Mater.* **10** 439–43
[2] Gheeraert E, Koizumi S, Teraji T, Kanda H and Nesládek M 2000 *Diamond Relat. Mater.* **9** 948–51
[3] Sque S J, Jones R, Goss J P and Briddon P R 2004 *Phys. Rev. Lett.* **92** 017402
[4] Cai Y, Zhang T, Anderson A B, Angus J C, Kostadinov L N and Albu T V 2006 *Diamond Relat. Mater.* **15** 1868–77
[5] Sakaguchi I, Gamo M N, Kikuchi Y, Yasu E, Haneda H, Suzuki T and Ando T 1999 *Phys. Rev.* B **60** R2139–41
[6] Teukam Z, Chevallier J, Saguy C, Kalish R, Ballutaud D, Barbe M, Jomard F, Tromson-Carli A, Cytermann C, Butler J E, Bernard M, Baron C and Deneuville A 2003 *Nat. Mater.* B **2** 482–6
[7] Koizumi S, Kamo M, Sato Y, Ozaki H and Inuzuka T 1997 *Appl. Phys. Lett.* **71** 1065–7
[8] Kato H, Yamasaki S and Okushi H 2005 *Appl. Phys. Lett.* **86** 222111
[9] Nesládek M 2005 *Semicond. Sci. Technol.* **20** R19
[10] Pinault M-A, Barjon J, Kociniewki T, Jomard F and Chevallier J 2007 *Physica* B **401** 51
[11] Casanova N, Tajani A, Gheeraert E, Bustarret E, Garrido J A, Nebel C E and Stutzmann M 2002 *Diamond Relat. Mater.* **11** 328–31
[12] Katagiri M, Isoya J, Koizumi S and Kanda H 2004 *Appl. Phys. Lett.* **85** 6365–7
[13] Kato H, Umezawa H, Tokuda N, Takeuchi D, Okushi H and Yamasaki S 2008 *Appl. Phys. Lett.* **93** 202103
[14] Koizumi S, Watanabe K, Hasegawa F and Kanda H 2001 *Science* **292** 1899–901
[15] Makino T, Tokuda N, Kato H, Kanno S, Yamasaki S and Okushi H 2008 *Phys. Status Solidi* a **205** 2200–6
[16] Worner E, Pleuler E, Wild C and Koidl P 2003 *Diamond Relat. Mater.* **12** 744–8
[17] Gajewski W, Achatz P, Williams O A, Haenen K, Bustarret E, Stutzmann M and Garrido J A 2009 *Phys. Rev.* B **79** 045206
[18] Nesládek M, Haenen K, D'Haen J, Koizumi S and Kanda H 2003 *Phys. Status Solidi* a **199** 77–81
[19] Lazea A, Mortet V, D'Haen J, Geithner P, Ristein J, D'Olieslaeger M and Haenen K 2008 *Chem. Phys. Lett.* **454** 310–3
[20] Koeck F A M, Nemanich R J, Lazea A and Haenen K 2009 *Diamond Relat. Mater.* **18** 789–91
[21] Teraji T, Arima K, Wada H and Ito T 2004 *J. Appl. Phys.* **96** 5906
[22] Bauer T, Schreck M, Hartwig J, Liu X H, Wong S P and Stritzker B 2006 *Phys. Status Solidi* a **203** 3056–62
[23] Kato H, Makino T, Yamasaki S and Okushi H 2007 *J. Phys. D: Appl. Phys.* **40** 6189
[24] Barjon J, Desfonds P, Pinault M-A, Kociniewski T, Jomard F and Chevallier J 2007 *J. Appl. Phys.* **101** 113701
[25] Barjon J, Pinault M-A, Kociniewski T, Jomard F and Chevallier J 2007 *Phys. Status Solidi* a **209** 2965

[26] Sauer R, Teofilov N, Thonke K and Koizumi S 2004 *Phys. Status Solidi* a **201** 2405
[27] Araujo D, Tajani A, Gheeraert E and Bustarret E 2004 *J. Phys.: Condens. Matter* **16** S287
[28] Ghodbane S, Omnès F, Bustarret E, Tavares C and Jomard F 2008 *Diamond Relat. Mater.* **17** 1324
[29] Lazea A, Barjon J, D'Haen J, Mortet V, D'Olieslaeger M and Haenen K 2009 *J. Appl. Phys.* **105** 083545
[30] van Enckevort W J P, Janssen G, Vollenberg W, Schermer J J, Giling L J and Seal M 1993 *Diamond Relat. Mater.* **2** 997
[31] Nishitani-Gamo M, Loh K P, Sakaguchi I, Takami T, Kusunoki I and Ando T 1999 *J. Vac. Sci. Technol.* A **17** 2991
[32] Battaile C C, Srolovitz D J and Butler J E 1998 *J. Cryst. Growth* **194** 353
[33] Habka N *et al* 2009 submitted
[34] BenMoussa A, Schuhle U, Scholze F, Kroth U, Haenen K, Saito T, Campos J, Koizumi S, Laubis C, Richter M, Mortet V, Theissen A and Hochedez J F 2006 *Meas. Sci. Technol.* **17** 913–7